Supporting Information for

Evaluating models for lithospheric loss and intraplate volcanism beneath the Central Appalachian Mountains

Maureen D. Long[1], Lara S. Wagner[2], Scott D. King[3], Rob L. Evans[4], Sarah E. Mazza[5], Joseph S. Byrnes[6,7], Elizabeth A. Johnson[8], Eric Kirby[9], Maximiliano J. Bezada[6], Esteban Gazel[10], Scott R. Miller[11], John C. Aragon[1,12], Shangxin Liu[3]

[1]Dept. Earth & Planetary Sciences, Yale University, New Haven, CT, USA
[2]Earth & Planets Laboratory, Carnegie Institution for Science, Washington, DC, USA
[3]Dept. Geosciences, Virginia Tech, Blacksburg, VA, USA
[4]Dept. Geology & Geophysics, WHOI, Woods Hole, MA, USA
[5]Dept. Geosciences, Smith College, Northampton, MA, USA
[6]Dept. Earth & Environmental Sciences, University of Minnesota, Minneapolis, MN, USA
[7]Dept. Geosciences, Northern Arizona University, Flagstaff, AZ, USA
[8]Dept. Geology & Environmental Science, James Madison University, Harrisonburg, VA, USA
[9]Dept. Geological Sciences, University of North Carolina at Chapel Hill, Chapel Hill, NC, USA
[10]Dept. Earth & Atmospheric Sciences, Cornell University, Ithaca, NY, USA
[11]Dept. Geology & Geophysics, University of Utah, Salt Lake City, UT, USA
[12]Now at: Earthquake Science Center, U.S. Geological Survey, Menlo Park, CA, USA

Contents of this file

Introduction

The supporting information contains supplemental data and methodology related to the analysis of topography and erosion rates above the Central Appalachian Anomaly.

Text S1
Analysis of topography and erosion rates above the Central Appalachian Anomaly
        To evaluate the relationships among topography, erosion rate, and substrate lithology in the central Appalachians, we compiled previously published erosion rates from ^{10}Be in modern sediment along tributaries in the three primary watersheds that drain the study area (Portenga &Bierman, 2011; Duxbury et al., 2015; Portenga et al., 2019). These data are considered to

represent basin-wide average erosion rates for the regions upstream of the sample (e.g., Granger et al., 1996; Bierman & Steig, 1996). We resampled 1-arc-second digital topographic data from the National Elevation Dataset to 3-arc-seconds for a nominal resolution of the final gridded topography of ~90m. These data were hydrologically conditioned and watersheds extracted in TopoToolbox, a suite of Matlab functions developed for geomorphic analyses (Schwanghart & Scherler, 2014). Channel longitudinal profiles were smoothed using quantile regression and the CRS algorithm of Schwanghart and Scherler (2017), using a smoothing parameter, K, of 10 and quantile, τ, of 0.5. Longitudinal profile smoothing was not extended across lithologic contacts or edges of features such as reservoirs, lakes, or dams in the medium-resolution National Hydrographic Dataset Plus version 2 (NHDPlus V2) data (https://www.epa.gov/waterdata/get-nhdplus-national-hydrography-dataset-plus-data).

To generate regional maps of channel steepness (Figure 7), the parameter k_{sn} was calculated on a pixel-by-pixel basis for all cells in the DEM with drainage areas greater than 1 km^2, using the equation

$$k_{sn} = S/A^{-\theta_{ref}} \qquad (S1)$$

where S is slope, A is drainage area, and θ_{ref} is a reference concavity. For this analysis, we used a $\theta_{ref} = 0.45$, following observations that this is a representative concavity for channels in the study area (Miller et al. 2013). Areas identified as lakes, reservoirs, and dams in the medium-resolution NHD, as well as a 0.5 km buffer around each, were removed from the grid of channel steepness. The channel steepness grid was smoothed with a Gaussian low-pass filter with a cutoff wavelength of 200 km (Greene et al., 2019). This smoothing length-scale was chosen as to fall within the range of preferred flexural wavelengths (170-280 km) associated with Plio-Pleistocene warping of the Orangeburg Escarpment (Moucha & Reutenik, 2017).

Within the 63 individual basins where erosion rates have been measured (Table S1), channel steepness values were calculated using the integral, or χ, method (Harkins et al. 2007; Perron and Royden, 2013) on unsmoothed channel profiles. Channel steepness was measured for the trunk stream and each tributary with a drainage area larger than 0.1 km^2, with the final value being the weighted average, where weighting is assigned by square of the channel length in χ coordinate. Channel profiles were visually inspected to evaluate the presence of slope-break knickpoints that might represent transient or non-equilibrium conditions (e.g., Kirby and Whipple, 2012). These were excluded (Table S1) from the final regression analysis of channel steepness and erosion rate (Figure 7).

To characterize lithologic substrate within these basins, geologic unit descriptions and contact locations were taken from Dicken et al. (2005) and Nicholson et al. (2005). The major lithology within each unit (GIS field "LITH1") was assigned to make a more generic rock classification that we utilize to classify points in Figures S1 and 7.

Linear regression of channel steepness and erosion rate was performed on both the complete (Figure S1) and the reduced data set (Figure 7) using a weighted bivariate regression that accounts for uncertainties in both variables (York et al., 2004). This regression adopts the methods of Thirumalai et al. (2011) and Trappitsch et al. (2018) for forcing the solution through the origin. The regression code and associated documentation are available on GitHub (https://github.com/scottrmiller/yorkregress_forced).
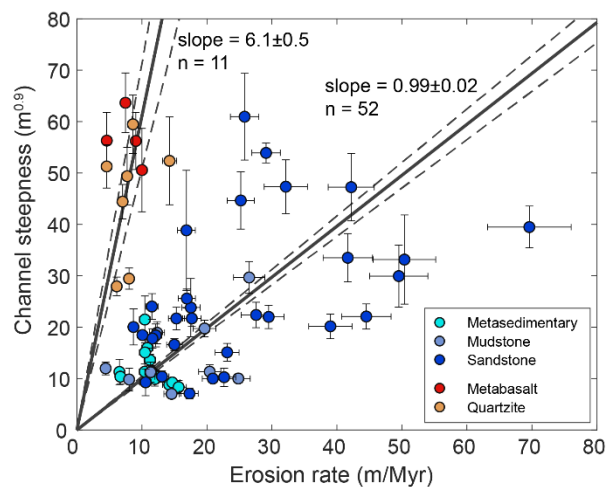
Figure S1

Figure S1. Channel steepness (k_{sn}) and erosion rate relationships for all basins in the study area.

Table S1

Table S1. Erosion rate sample locations and watershed metrics from upstream basins.

Basin ID[A]	Drainage basin[B]	Easting (m)[C]	Northing (m)	Elevation (m)	Dominant rock	Erosion rate (m/Myr)	k_{sn} ($m^{0.9}$)	Area (km)	Equilibrium flag[D]
JSQ100	Susq.	738047	4584417	296	Sandstone	32.14 ± 3.34	47.3 ± 5.2	3.0	1
JSQ102	Susq.	737789	4593594	346	Sandstone	69.6 ± 6.43	39.5 ± 4.1	3.3	0
JSQ103	Susq.	734633	4608264	386	Sandstone	41.67 ± 3.81	33.5 ± 4.7	5.7	1
JSQ104	Susq.	746512	4621169	544	Sandstone	39 ± 3.33	20.2 ± 2.4	3.6	1
JSQ105	Susq.	714656	4592882	549	Sandstone	22.65 ± 1.78	10.3 ± 1.8	3.1	1
JSQ106	Susq.	720585	4591886	492	Sandstone	27.57 ± 2.3	22.4 ± 2.5	3.2	1
JSQ107	Susq.	720688	4589638	437	Sandstone	44.52 ± 3.81	22.1 ± 2.4	3.3	1
JSQ108	Susq.	720962	4586067	499	Sandstone	17.68 ± 1.42	21.7 ± 1.6	5.2	0
JSQ109	Susq.	741377	4609163	474	Sandstone	50.39 ± 4.8	33.2 ± 8.7	3.3	1
JSQ111	Susq.	754584	4593323	372	Sandstone	16.85 ± 1.37	38.8 ± 11.7	5.6	0
JSQ112	Susq.	754952	4586030	342	Sandstone	49.52 ± 4.48	29.9 ± 6	3.4	0
JSQ113	Susq.	753434	4582971	445	Sandstone	23.11 ± 1.83	15.1 ± 1.7	3.8	1
JSQ114	Susq.	728079	4569483	574	Sandstone	13.09 ± 1.08	10.4 ± 1.1	6.4	1
JSQ115	Susq.	731860	4573171	481	Sandstone	17.53 ± 1.42	23.8 ± 5.7	4.7	0
JSQ116	Susq.	748293	4565600	415	Sandstone	15.3 ± 1.22	21.7 ± 2.2	6.5	1
JSQ117	Susq.	748673	4565921	420	Sandstone	15 ± 1.21	16.6 ± 1.2	3.3	1
JSQ118	Susq.	768837	4575357	328	Sandstone	25.8 ± 2.19	61 ± 8.4	4.0	0

JSQ119	Susq.	770757	4574247	368	Sandstone	42.2 ± 3.54	47.2 ± 6.5	5.6	1
JSQ120	Susq.	758110	4566515	287	Sandstone	25.21 ± 2.1	44.7 ± 5.6	15.5	0
JSQ123	Susq.	768474	4566321	580	Sandstone	11.62 ± 0.94	17.8 ± 1.9	2.6	1
JSQ124	Susq.	806851	4568033	211	Mudstone	12.33 ± 1.15	18.9 ± 2.2	2.6	1
JSQ125	Susq.	815274	4556335	377	Sandstone	29.5 ± 2.35	22 ± 2.3	9.8	0
JSQ126	Susq.	812940	4554905	507	Sandstone	20.91 ± 1.61	10 ± 0.5	2.2	1
JSQ127	Susq.	810155	4553009	511	Sandstone	10.57 ± 0.85	9.3 ± 2.6	5.5	1
JSQ128	Susq.	826250	4554266	433	Sandstone	16.91 ± 1.33	25.6 ± 1.8	3.2	1
JSQ130	Susq.	868285	4556417	165	Mudstone	14.56 ± 1.18	7 ± 0.6	6.1	1
JSQ131	Susq.	876224	4556798	193	Mudstone	19.64 ± 1.76	19.7 ± 1.6	5.2	1
JSQ132	Susq.	861111	4531129	167	Mudstone	8.03 ± 0.68	9.8 ± 2.2	4.0	1
JSQ133	Susq.	860361	4494424	407	Sandstone	10.08 ± 0.81	18.5 ± 0.8	3.0	1
JSQ134	Susq.	846587	4512145	137	Mudstone	20.43 ± 1.71	11.3 ± 1.3	5.5	1
JSQ135	Susq.	842081	4504952	128	Mudstone	24.83 ± 1.84	10 ± 0.9	4.2	0
JSQ136	Susq.	783865	4474081	265	Mudstone	4.42 ± 0.39	12 ± 1.2	3.0	1
JSQ140	Susq.	750828	4468137	371	Sandstone	8.7 ± 0.74	20 ± 3.5	3.3	1
JSQ141	Susq.	745434	4468675	393	Sandstone	11.54 ± 0.95	24 ± 2.5	4.6	0
JSQ142	Susq.	728770	4480379	284	Mudstone	11.34 ± 0.91	11.2 ± 2	2.7	1
JSQ143	Susq.	770107	4509898	397	Quartzite	6.12 ± 0.52	27.9 ± 1.8	3.6	0
JSQ144	Susq.	771083	4514664	503	Quartzite	8.02 ± 0.67	29.5 ± 2.1	3.1	1
JSQ146	Susq.	797099	4526095	517	Sandstone	17.32 ± 1.34	7.1 ± 1.1	3.1	1
JSQ149	Susq.	776948	4545630	250	Mudstone	26.5 ± 2.39	29.7 ± 3.1	3.0	1
JSQ150	Susq.	899798	4417344	67	Metasedimentary	11.25 ± 0.9	13.6 ± 1.1	4.0	0
JSQ151	Susq.	898866	4417918	112	Metasedimentary	6.54 ± 0.56	11.3 ± 2.5	3.4	1
JSQ152	Susq.	898393	4417641	133	Metasedimentary	6.69 ± 0.61	10.4 ± 1.5	3.1	1
JSQ153	Susq.	911843	4419808	131	Metasedimentary	14.67 ± 1.17	9.3 ± 0.5	25.5	1
JSQ154	Susq.	898883	4420059	67	Metasedimentary	10.45 ± 0.84	21.5 ± 4.6	5.3	0
JSQ155	Susq.	898616	4423299	113	Metasedimentary	10.85 ± 0.87	16 ± 2.3	4.0	1
JSQ156	Susq.	882950	4426180	188	Metasedimentary	12.14 ± 0.97	10.4 ± 1.2	4.3	1
JSQ157	Susq.	891136	4409935	149	Metasedimentary	15.65 ± 1.18	8.3 ± 1.3	4.0	1
JSQ158	Susq.	886018	4412505	149	Metasedimentary	11.44 ± 0.9	11.4 ± 1.1	6.9	1
JSQ159	Susq.	875031	4415483	236	Metasedimentary	10.44 ± 0.85	11.3 ± 1.5	7.6	1
JSQ160	Susq.	872188	4416384	214	Metasedimentary	12.01 ± 0.96	9.9 ± 1.4	3.7	1
JSQ161	Susq.	886824	4430423	126	Metasedimentary	10.47 ± 0.86	15.1 ± 3	3.4	0
POT18	Pot.	818514	4346631	119	Metasedimentary	14.2 ± 1.06	8.8 ± 0.5	13.5	1
POT45	Pot.	661008	4269318	703	Sandstone	29.1 ± 2.2	53.9 ± 1.9	29.4	1
POT64	Pot.	734901	4408831	217	Sandstone	12.15 ± 0.93	18.4 ± 2.2	12.6	1
SH02	Pot.	730110	4282751	380	Metabasalt	9.06 ± 0.75	56.2 ± 5.6	4.1	1
SH04	Pot.	693189	4230179	429	Quartzite	4.58 ± 0.79	51.3 ± 4.2	13.6	0
SH18	Pot.	730112	4282749	380	Metabasalt	4.6 ± 0.39	56.3 ± 5.5	4.1	1
SH26	James	708069	4241013	619	Metabasalt	10.01 ± 0.79	50.6 ± 8.1	2.6	1
SH31	Pot.	692434	4225858	482	Quartzite	7.03 ± 0.57	44.4 ± 3.3	8.5	0
SH37	Pot.	697284	4236291	464	Quartzite	7.74 ± 0.62	49.4 ± 5.6	1.5	1

SH39	Pot.	694143	4232771	512	Quartzite	8.62 ± 0.82	59.5 ± 5.7	3.1	1
SH40	James	702052	4234759	568	Metabasalt	7.47 ± 0.61	63.7 ± 5.8	3.3	0
SH54	Pot.	699080	4240433	496	Quartzite	14.25 ± 1.1	52.4 ± 8.6	1.8	1

[A] JSQ samples from Portenga and Bierman (2011). POT samples from Portenga et al. (2019). SH samples from Duxbury et al. (2015).
[B] Abbreviations: Susquehanna (Susq.), Potomac (Pot.)
[C] UTM Zone 17
[D] Denotes whether channel profiles from basin above sample are consistent with topographic equilibrium (1) or whether these display non-equilibrium characteristics (0)

Supplementary References

Bierman, P., & Steig, E.J. (1996). Estimating rates of denudation using cosmogenic isotope abundances in sediment. *Earth Surface Processes and Landforms, 21,* 125-139.

Dicken, C.L., Nicholson, S.W., Horton, J.D., Kinney, S. A., Gunther, Gregory, Foose, M. P., & Mueller, J. A. L. (2005). Preliminary integrated geologic map databases for the United States: Delaware, Maryland, New York, Pennsylvania, and Virginia: U.S. Geological Survey Open File Report 2005-1325, accessed January 31, 2013, at http://pubs.usgs.gov/of/2005/1325/

Duxbury, J., Bierman, P. R., Portenga, E. W., Pavich, M. J., Southworth, S., & Freeman, S. P. (2015). Erosion rates in and around Shenandoah National Park, Virginia, determined using analysis of cosmogenic 10Be. *American Journal of Science*, *315*(1), 46-76. https://doi.org/10.2475/01.2015.02

Granger, D.E., Kirchner, J.W., & Finkel, R. (1996). Spatially averaged long-term erosion rates measured from in situ-produced cosmogenic nuclides in alluvial sediment. *Journal of Geology, 104,* 249-257.

Greene, C. A., Thirumalai, K., Kearney, K. A., Delgado, J. M., Schwanghart, W., Wolfenbarger, N. S., & Blankenship, D. D. (2019). The climate data toolbox for MATLAB. *Geochemistry, Geophysics, Geosystems*, *20*(7), 3774-3781. https://doi.org/10.1029/2019GC008392

Harkins, N., Kirby, E., Heimsath, A., Robinson, R., & Reiser, U. (2007). Transient fluvial incision in the headwaters of the Yellow River, northeastern Tibet, China. *Journal of Geophysical Research: Earth Surface*, *112*(F3). https://doi.org/10.1029/2006JF000570

Miller, S. R., Sak, P. B., Kirby, E., & Bierman, P. R. (2013). Neogene rejuvenation of central Appalachian topography: Evidence for differential rock uplift from stream profiles and erosion rates. *Earth and Planetary Science Letters*, *369*, 1-12. https://doi.org/10.1016/j.epsl.2013.04.007

Moucha, R., & Ruetenik, G. A. (2017). Interplay between dynamic topography and flexure along the US Atlantic passive margin: Insights from landscape evolution modeling. *Global and Planetary Change*, *149*, 72-78. https://doi.org/10.1016/j.gloplacha.2017.01.004

Nicholson, S. W. D., Horton, C. L., Labay, J. D., Foose, K. A., Mueller, M. P., & Julia, A. L. (2005). Preliminary integrated geologic map databases for the United States: Kentucky, Ohio, Tennessee, and West Virginia: U.S. Geological Survey Open File Report 2005-1324, accessed January 31, 2013, at http://pubs.usgs.gov/of/2005/1324

Perron, J. T., & Royden, L. (2013). An integral approach to bedrock river profile analysis. *Earth Surface Processes and Landforms*, *38*(6), 570-576. https://doi.org/10.1002/esp.3302

Portenga, E. W., & Bierman, P. R. (2011). Understanding Earth's eroding surface with 10 Be. *GSA today*, *21*(8), 4-10. http://doi.org/10.1130/G111A.1

Portenga, E. W., Bierman, P. R., Trodick, C. D., Greene, S. E., DeJong, B. D., Rood, D. H., & Pavich, M. J. (2019). Erosion rates and sediment flux within the Potomac River basin quantified over millennial timescales using beryllium isotopes. *GSA Bulletin*, *131*(7-8), 1295-1311. https://doi.org/10.1130/B31840.1

Schwanghart, W., & Scherler, D. (2014). TopoToolbox 2–MATLAB-based software for topographic analysis and modeling in Earth surface sciences. *Earth Surface Dynamics*, *2*(1), 1-7. https://doi.org/10.5194/esurf-2-1-2014

Schwanghart, W., & Scherler, D. (2017). Bumps in river profiles: uncertainty assessment and smoothing using quantile regression techniques. *Earth Surface Dynamics*, *5*, 821-839. https://doi.org/10.5194/esurf-5-821-2017

Thirumalai, K., A. Singh, and R. Ramesh (2011), A MATLAB code to perform weighted linear regression with (correlated or uncorrelated) errors in bivariate data, Journal of the Geological Society of India, 77(4), 377-380. https://doi.org/10.1007/s12594-011-0044-1

Trappitsch, R., Boehnke, P., Stephan, T., Telus, M., Savina, M. R., Pardo, O., Davis, A.M., Dauphas, N., Pellin, M.J., & Huss, G. R. (2018). New constraints on the abundance of 60Fe in the early solar system. The Astrophysical Journal Letters, 857(2), L15. http://doi.org/10.3847/2041-8213/aabba9

York, D., Evensen, N. M., Martınez, M. L., & De Basabe Delgado, J. (2004). Unified equations for the slope, intercept, and standard errors of the best straight line. *American Journal of Physics*, 72(3), 367-375. https://doi.org/10.1119/1.1632486